European Conference on Computational Fluid Dynamics
ECCOMAS CFD 2006
P. Wesseling, E. Oñate and J. Périaux (Eds)

COMPUTATION OF MODAL RADIATION THROUGH AN ENGINE EXHAUST ON ADAPTIVELY REFINED MESHES

Xun Huang, Zhaokai Ma and Xin Zhang

Aeronautics and Astronautics
University of Southampton
Southampton, SO 17 1BJ, UK
e-mail: {xunger,mazhk,x.zhang1}@soton.ac.uk

Key words: Duct acoustics, Aeroengine, Adaptive mesh refinement, Computational aeroacoustics, Linearised Euler equations, Acoustic perturbation equations

Abstract. *This paper outlines a computational method for spinning modal acoustic propagation and radiation through an aeroengine exhaust duct and core nozzle, using adaptive refined mesh (AMR) with the aim of improving the computational efficiency. To allow the computation with solid boundaries of a general aircraft engine, the method is extended to support body-fitted multi-blocks AMR. Propagation inside the duct, diffraction at the lip of the duct and propagation into the near field is modelled by the linearised Euler equations, which admit hydrodynamic instabilities in the exhaust mean flow. In order to suppress this type of instabilities, the acoustic perturbation equations are also used, which have been extended to the cylindrical coordinates. The suitability of the governing equations and the quality of the proposed AMR method are validated through a case study of single spinning mode radiation from a generic engine bypass duct.*

1 Introduction

The development of high bypass ratio turbofan engines has led to more prominent tonal noise, which is generated by the fan assembly. An accurate model of the propagation of tonal noise within and away from the engine would prove a valuable tool in determining ways to alleviate the fan tone noise problem. In the case of radiation from either a bypass duct or a core exhaust nozzle, as shown in Fig. 1, there are issues associated with the presence of a mean flow with a shear layer between the exhaust flow and the external stream. Refractive effects due to the presence of the shear flow change noise radiation pattern. The physical process of noise generation and radiation is governed by the Navier-Stokes equations. At present, a full numerical solution of noise generation, propagation and radiation process using the Navier-Stokes equations is not feasible. However, certain aspects of the noise propagation and radiation process can be modelled by linearised equations. For example, in the duct downstream of the rotor-stator region of an aeroengine, where nonlinear and viscous noise generation effects are minimal, the propagation of the rotor-stator noise can be studied using the inviscid linearised equations about the mean flow. Computational aeroacoustics (CAA) methods based upon the Euler or linearsied Euler equations (LEE) are general in terms of governing physics,[1] whereas its realistic engineering applications are generally expensive and call for continuous research into efficient computational schemes/methods.

Adaptive mesh refinement (AMR) is efficient and effective in treating problems with multiple spatial and temporal scales.[2] It represents the computational domain as hierarchal refinement levels and increases the grids resolution only in areas of interest. Consequently the computational efficiency is improved by reducing the number of computational cells. The operation of refinement could be operated either on the fine-grained cells level,[2] i.e. cell-based structured AMR, or on the coarse-grained blocks level,[3,4] which is termed as block-based structured AMR. It is well accepted that block-based AMR requires less programming efforts and is computationally more effective than cell-based AMR in terms of communication costs and memory requirements. In our earlier work[5] a block-structured AMR code was constructed and tested against benchmark problems on rectangular meshes. The subsequent efforts extended the code to work on a distributed-memory parallel machine[6] using message passing interface (MPI) library, and supported body-fitted meshes to solve aeroacoustic problems of practical significance, e.g. acoustic radiation from a general aeroengine intake.[7] The elements of the employed AMR algorithms, its flexibility and efficiency have been discussed.[5–7]

Block-structured AMR has been applied to study the radiation of spinning modes from a unflanged duct and aeroengine intake problems to establish far-field directivity.[5,7] Results were verified by comparing to analytical solutions and others' FEM and LEE solutions. In this work the block-structured AMR is applied to the general case of noise radiation from realistic high bypass engine exhaust geometry with mean flow. A computational model used to determine the propagation and radiation of acoustic waves is outlined. The computational scheme described here allows acoustic waves, propagating inside the bypass duct of a generic aircraft engine, to be admitted into a computational domain that comprises the aft duct section, the exit plane of the duct, and the jet flow immediately downstream. The wave admission is realised through an absorbing non-reflecting boundary treatment which admits incoming waves and damps spurious waves generated by the numerical solutions. The exhaust geometry is assumed axisymmetric and the mean flow axisymmetric with no swirl component. The acoustic disturbances are represented by a Fourier series in the circumferential direction. For a particular circumferential mode, a simplified system of equations were formulated, termed the 2.5D form of the LEE.[8] Subsequently, The wave propagation and diffraction were calculated with LEE, using a range of high-order schemes.[9]

The hydrodynamic shear layer instabilities induce unstable solutions in the LEE computation, corrupting the desired acoustic solutions. To stabilize the LEE solutions, it is a common practice to remove some mean shear terms in the governing equations. The approach was validated against Munt's analytical solution of semi-infinite duct radiation problem[10] in the previous work.[8,9] However, further tests against other comparable methods are necessary on realistic geometry and flow conditions. The acoustic perturbation equations (APE),[11] which have been extended to the cylindrical coordinates for the aero-engine case, are also used in this work to suppress instabilities. The APE solutions are compared to the previous LEE solutions[9] through a case study of the radiation of single spinning mode from a generic engine bypass duct. The far-field directivity is estimated via an integral surface solution of the Ffowcs Williams and Hawkings (FW-H) equation.[12]

2 The Block-structured AMR Algorithm

The existing AMR applications[3,13] generally employ a block-structured AMR algorithm. It involves a) representing the two-dimensional (2D)/ three-dimensional (3D) hierarchical computational domain in blocks, b) connecting the generated blocks in a quadtree/octree data structure, c) estimating local truncation errors at all grid points and identifying blocks with excessive errors, d) regridding the identified blocks by superimposing or removing blocks to accommodate changes in flow physics, and e) redistributing computational load between processors to maintain dynamic load balancing. This procedure is operated recursively until either a given refinement/coarsening level is reached or a predefined local truncation error level has been met. After regridding, the initial conditions of the newly generated blocks are inherited from their base blocks. This operation is referred to as the AMR prolongation operation. Conversely, after each computing step, the solutions on the finer blocks should be used to update the solutions of the corresponding base blocks to maintain the desired accuracy. This is known as the AMR restriction operation. To provide partial differences of variables in cells located near a block boundary, an extra area surrounding each block is required. This operation is referred to as the ghost construction. More detailed descriptions of the AMR framework were given in the previous work.[5,7] They are not repeated here for the sake of brevity.

3 Numerical Methods

3.1 Governing Equations

The 2.5D form of LEE is firstly given to make the paper complete. Assuming small perturbations about a steady mean flow, acoustic wave propagation can be described by the linearized Euler equations in a cylindrical coordinate system. If the acoustic disturbances are restricted to the multiples of the blade passing frequency and propagate on an axisymmetric mean flow field without swirl, it is possible to write the disturbances in terms of a Fourier series, e.g. for the pressure disturbance p' at a single frequency k the series is

$$p' = \sum_{m=0}^{\infty} p'_m(x,r)e^{[i(kt-m\theta)]}, \tag{1}$$

where x is the axial coordinate, r the radial coordinate, t is time, m is the circumferential mode and θ the circumferential angle. Consequently, there are two important relations for the circumferential velocity disturbance w' and the pressure disturbance p' correspondingly. They are

$$\frac{\partial w'}{\partial \theta} = -\frac{m}{k}\frac{\partial w'}{\partial t}, \qquad \frac{\partial^2 p'}{\partial t \partial \theta} = mkp'. \tag{2}$$

By using Eqs. (2) the general LEE in the cylindrical coordinates could be simplified to a set of equations that are generally called 2.5D LEE equations.[5] The complete governing equations in the cylindrical coordinates for a single blade passing frequency k are:

$$\begin{aligned}
\frac{\partial \rho'}{\partial t} + \frac{\partial(\rho' u_0 + \rho_0 u')}{\partial x} + \frac{\partial(\rho' v_0 + \rho_0 v')}{\partial r} - \frac{m\rho_0}{kr}w'_t + \frac{\rho' v_0 + \rho_0 v'}{r} &= 0, \\
\frac{\partial u'}{\partial t} + u_0\frac{\partial u'}{\partial x} + v_0\frac{\partial u'}{\partial r} + (u' + \frac{\rho'}{\rho_0}u_0)\frac{\partial u_0}{\partial x} + (v' + \frac{\rho'}{\rho_0}v_0)\frac{\partial u_0}{\partial r} + \frac{\partial p'}{\rho_0 \partial x} &= 0, \\
\frac{\partial v'}{\partial t} + u_0\frac{\partial v'}{\partial x} + v_0\frac{\partial v'}{\partial r} + (u' + \frac{\rho'}{\rho_0}u_0)\frac{\partial v_0}{\partial x} + (v' + \frac{\rho'}{\rho_0}v_0)\frac{\partial v_0}{\partial r} + \frac{\partial p'}{\rho_0 \partial r} &= 0, \\
\frac{\partial w'_t}{\partial t} + u_0\frac{\partial w'_t}{\partial x} + v_0\frac{\partial w'_t}{\partial r} + \frac{mk}{\rho_0 r}p' + \frac{w'_t v_0}{r} &= 0,
\end{aligned} \tag{3}$$

where superscript ($'$) and subscript (0) denote perturbation and mean properties respectively; u' and v' are velocity perturbations in the x and r directions respectively; $w'_t = \partial w'/\partial t$. The fluid is modelled as a perfect gas. $p' = C_0^2\rho'$, where C_0 is sound speed. The boundary treatment for w'_t is the same as that for w'.

For the cases with a shear layer, LEE also admits hydrodynamic instabilities, which can lead to overwhelm the desired acoustic solutions. In order to suppress this type of unbounded growth of instabilities, a set of APE have been proposed to the computation of the acoustic wave convection and refraction in Cartesian coordinates. An in-depth discussion of the relevant theoretical background can be found in Ewert & Schr's work.[11] In this work they are extended to the cylindrical coordinates, according to the APE-2 system,[11] take the form as follows:

$$\begin{aligned}
\frac{\partial \rho'}{\partial t} + \frac{\partial(\rho' u_0 + \rho_0 u')}{\partial x} + \frac{\partial(\rho' v_0 + \rho_0 v')}{\partial r} - \frac{m\rho_0}{kr}w'_t + \frac{\rho' v_0 + \rho_0 v'}{r} &= 0, \\
\frac{\partial u'}{\partial t} + \frac{\partial(u_0 u' + v_0 v')}{\partial x} + \frac{\partial p'}{\rho_0 \partial x} + \frac{\gamma\rho'}{\rho_0}(u_0\frac{\partial u_0}{\partial x} + v_0\frac{\partial u_0}{\partial r}) &= 0, \\
\frac{\partial v'}{\partial t} + \frac{\partial(u_0 u' + v_0 v')}{\partial r} + \frac{\partial p'}{\rho_0 \partial r} + \frac{\gamma\rho'}{\rho_0}(u_0\frac{\partial v_0}{\partial x} + v_0\frac{\partial v_0}{\partial r}) &= 0, \\
\frac{\partial w'_t}{\partial t} + u_0\frac{\partial w'_t}{\partial x} + v_0\frac{\partial w'_t}{\partial r} + \frac{mk}{\rho_0 r}p' + \frac{w'_t v_0}{r} &= 0,
\end{aligned} \tag{4}$$

where the first and last equations of Eqs. (3) are kept, and the definitions of variables are the same as in Eqs. (3).

3.2 Numerical Schemes

A number of numerical issues associated with AMR on CAA applications are addressed in the foregoing work as well. The numerical part consists of 4^{th}-order spatial[14,15] and temporal schemes,[16] 2^{nd}- to 6^{th}-order interpolations, 4^{th}-order artificial selective damping[14] and 10^{th}-order explicit filter.[17] The working of a high-order spatial scheme on an adaptively refined mesh was indicated and spectral analysis proved the steady stability of the employed spatial schemes,[5] while pseudospectra analysis[18] provided transient properties under an AMR environment. In the ghost construction operation, several interpolation methods (a 2^{nd}- and a 4^{th}-order linear interpolation and a 6^{th}-order polynomial interpolation) have been tested in the previous work.[7] It was found that combined with 4^{th}-order spatial schemes and 6^{th}-order interpolations, the convergence rate was around 3.7.

3.3 Curvilinear Coordinate System

In an earlier work[6] it was shown that a Cartesian mesh with low-order immersed boundary method[19] performed much poorly than a body-fitted mesh to solve acoustic propagation problems with curved geometries. There are also some other attempts of using AMR for body-fitted multi-blocks meshes,[13,20] where curved geometries were allowed to be transformed into and simulated using a uniform computational domain. This can be achieved by using the coordinate transformation given by Eqs. (5-7), which represent a transformation from the physical to the computational coordinates. For simplicity the time variance of both coordinate systems is not considered.

$$\xi = \xi(x,r), \qquad \eta = \eta(x,r). \tag{5}$$

The first order spatial derivatives of the governing equations are evaluated using the chain rule:

$$\begin{aligned} \frac{\partial}{\partial x} &= \frac{\partial \xi}{\partial x}\frac{\partial}{\partial \xi} + \frac{\partial \eta}{\partial x}\frac{\partial}{\partial \eta}, \\ \frac{\partial}{\partial r} &= \frac{\partial \xi}{\partial r}\frac{\partial}{\partial \xi} + \frac{\partial \eta}{\partial r}\frac{\partial}{\partial \eta}, \end{aligned} \tag{6}$$

with the transformation metrics defined as

$$\begin{aligned} \frac{\partial \xi}{\partial x} &= J\left(\frac{\partial r}{\partial \eta}\right), \qquad \frac{\partial \xi}{\partial r} = J\left(-\frac{\partial x}{\partial \eta}\right), \\ \frac{\partial \eta}{\partial x} &= J\left(-\frac{\partial r}{\partial \xi}\right), \qquad \frac{\partial \eta}{\partial r} = J\left(\frac{\partial x}{\partial \xi}\right). \end{aligned} \tag{7}$$

J is the transformation Jacobian relating the geometric properties of the physical space to the uniform computational space and is given by

$$J = \left[\frac{\partial x}{\partial \xi}\frac{\partial r}{\partial \eta} - \frac{\partial x}{\partial \eta}\frac{\partial r}{\partial \xi}\right]^{-1}. \tag{8}$$

4 Noise Radiation from an Aeroengine Exhaust Duct

In this case the aforementioned 4^{th}-order explicit schemes,[15] the 4^{th}-order 4-6 LDDRK[16] temporal scheme, the 4^{th}-order linear interpolation and the 10^{th}-order filter[17] are employed. The setup and discussions of the case problem are given below.

4.1 Setup

The basic problem is illustrated in Figs. 2-3 that show the computational domain on which the near-field CAA propagation calculation is performed. The specific configuration resembles the previous effort.[9] The illustrated background mean flow is in terms of Mach number, which is set to 0.338 at the inflow boundary inside the duct. The exhaust stream is issued into a stationary environment. Inside the duct, a buffer zone[21] is used to absorb the reflective spurious waves as well as to accommodate incoming modal waves, which are defined as follows:

$$
\begin{aligned}
\rho'(x,r,\theta,t) &= a[J_m(k_r r) + c_1 Y_m(k_r r)]\cos(kt - k_a x - m\theta), \\
u'(x,r,\theta,t) &= \frac{k_a}{k - k_a M_j} p', \\
v'(x,r,\theta,t) &= -\frac{a}{k - k_a M_j}\frac{\mathrm{d}[J_m(k_r r) + c_1 Y_m(k_r r)]}{\mathrm{d}r}\sin(kt - k_a x - m\theta), \\
{w_t}'(x,r,\theta,t) &= -\frac{amk[J_m(k_r r) + c_1 Y_m(k_r r)]}{r(k - k_a M_j)}\sin(kt - k_a x - m\theta), \\
w'(x,r,\theta,t) &= \frac{am}{r(k - k_a M_j)}[J_m(k_r r) + c_1 Y_m(k_r r)]\cos(kt - k_a x - m\theta), \\
p'(x,r,\theta,t) &= a[J_m(k_r r) + c_1 Y_m(k_r r)]\cos(kt - k_a x - m\theta),
\end{aligned}
\tag{9}
$$

where M_j is nondimensional velocity inside the duct; a is fixed at 10^{-4} to ensure small relative changes in density (as required for LEE and APE solutions); J_m and Y_m are the m^{th} order Bessel functions of the first and second kind respectively; k_a is the axial wave number and k_r is the radial wave number. k_r is the n^{th} solution of the following equation determined by the hard-wall boundary conditions of the duct

$$
\frac{\mathrm{d}[J_m(y_{outer}k_r)]}{\mathrm{d}r}\frac{\mathrm{d}[Y_m(y_{inner}k_r)]}{\mathrm{d}r} - \frac{\mathrm{d}[J_m(y_{inner}k_r)]}{\mathrm{d}r}\frac{\mathrm{d}[Y_m(y_{outer}k_r)]}{\mathrm{d}r} = 0, \tag{10}
$$

where y_{outer} and y_{inner} are the height of the bypass duct inner wall and the inner hub radius. k_a is calculated from

$$
k_a = \frac{k}{1 - M_j^2}\left(-M_j \pm \sqrt{1 - \frac{k_r^2(1 - M_j^2)}{k^2}}\right), \tag{11}
$$

the selection of plus or minus ($\pm$) signs in the parenthesis is determined by the propagation direction of the spinning wave, e.g. plus (+) is for the positive propagation direction in the axial coordinate, and vice versa. The constant c_1 satisfies the following relations

$$c_1 = \frac{\frac{\mathrm{d}}{\mathrm{d}r}[J_m(y_{outer}k_r)]}{\frac{\mathrm{d}}{\mathrm{d}r}[Y_m(y_{outer}k_r)]} \tag{12}$$

and

$$c_1 = \frac{\frac{\mathrm{d}}{\mathrm{d}r}[J_m(y_{inner}k_r)]}{\frac{\mathrm{d}}{\mathrm{d}r}[Y_m(y_{inner}k_r)]}. \tag{13}$$

In the case four radial modes are solved in the incoming waves. They are summarised in Table 1. A buffer zone is also placed around the outer boundaries of the domain and

n	$f(Hz)$	k	k_r	k_a
1	1562.7	28.3179	10.60	19.11
2	1562.7	28.3179	14.01	17.49
3	1562.7	28.3179	16.50	15.93
4	1562.7	28.3179	19.71	13.35

Table 1: Summary of the Incoming Waves, $m = 13$, $k = 28.3179$.

inside the core exhaust nozzle. The target solutions of this buffer zone is set to zero to absorb spurious numerical reflections.

The far-field directivity is estimated through an integral solution of FW-H equations.[12] For simplicity the FW-H integral surface shown in Fig. 3 is located at the borders of blocks surrounding the engine exhaust. The far-field observers are located at 100m from the conical rear of the exhaust geometry.

4.2 Discussions of AMR Operations

AMR could provide higher computational efficiency and more flexibility than a uniform mesh. Fig. 4 illustrates the procedure of the adaptively refined mesh as acoustic waves propagate and radiate out of the engine exhaust. The outer buffer zone is not displayed. The total number of grid points increases from $36,000$ to $180,000$. The computation

Grids	$t = 1$	$t = 2$	$t = 5$	$t = 8$
AMR	1478s	3401s	13460s	26670s
Uniform mesh	3971s	8002s	20120s	31920s

Table 2: The computation time of the prediction at t.

is executed and tested on a computer with a Pentium IV 3.0GHz CPU and 2GBytes memory. Table 2 shows that the computation time of AMR is increased along with the increase of grid points. In the initial stage (i.e. $t < 5$) the computation time of AMR is around 100% faster than the computation time on the uniform mesh. After that, the computational efficiency of AMR gradually decreases. Finally it reaches the same level of the computational efficiency on the uniform mesh, due to the extended span of the acoustic wave in the whole computational domain (see Fig. 4(d)), where the adaptively regridding operation is no use anymore.

4.3 Near-Field Propagation

Fig. 5 compares the near-field waves propagation computed by both LEE and APE, respectively. The computation is performed on a mesh adaptively refined as the acoustic propagation. Two refinement levels are used. The coarse level mesh consistes of $36,000$ grid points, while the fine level mesh is adaptively updated and the number of grid points varies accordingly. In this case, after $t = 12$, hydrodynamic instabilities developed in the shear layer are evident with the LEE method (see Fig. 5(a)). These instability waves that can not be suppressed neither by filtering nor by multigrid prolongation develop to overwhelm the desired acoustic solutions completely. Since APE are claimed to be stable for arbitrary mean flow fields,[11] Eqs. (4) are applied to the case. Fig. 5(b) shows perturbation pressure contours computed by the APE method. It indicates that the numerical instabilities are avoided, whereas the near-field propagation pattern retains the same key features as the LEE solutions: wave diffraction off the lip of the bypass duct and reflections off the surface of the afterbody of the engine exhaust. It should be noted that, for the present test case computation, the mean flow conditions in the core nozzle are the same as those in the bypass duct. Upstream traveling waves now appear inside the core nozzle and are visible in Fig. 5(b).

Fig. 6 shows the near-field sound pressure level, $\text{SPL} = 20\log_{10}(p'_{rms}/(2\times 10^{-5}))$, where the selected time to compute p'_{rms} satisfies $t < 12$, in which the hydrodynamic instabilities appeared in the LEE computation still do not overwhelm the acoustic solutions. It shows that propagation patterns predicted by the both methods agree well in most parts, whereas the sound pressure level of APE is a bit higher at high and low angles than the LEE prediction. By using the APE method, several other spinning mode waves, i.e. $n = 2-4$, are solved as well. Fig. 7 displays the results of the perturbation pressure and sound pressure level contours.

4.4 Far-Field Directivity

Through an integral surface solution of the FW-H equation, the far-field directivities of the four spinning mode radiation are predicted based on the near-field APE solutions. The outcomes are compared with the LEE prediction[9] in Fig. 8, respectively. To avoid the potential effect of the hydrodynamic instabilities in the computation with LEE method, the time series satisfying $t < 12$ was used in the LEE computation. The limit is avoided in the APE computation. Results in Fig. 8 show that the two patterns predicted by the APE solutions and the LEE solutions are similar. The main peak angel and the peak level of the APE prediction match the LEE solutions well. The differences in the peak radiation level between APE results and LEE results are less than 0.5dB, whereas the peak radiation angles differ form each other by less than 1.4 deg. In other parts of the directivity, the patterns are also similar. Nevertheless, the shape of the APE results is generally smoother than the curve of the LEE results. It implies that in this case the APE may introduce some kind of dissipations, which operate to suppress hydrodynamic instabilities. Another finding is that the amplitude of APE results is generally higher than that of LEE results. In Fig. 6 the same finding is displayed. Here the maximal difference appears in the case of $n = 4$, where the difference at the high angles ($\phi > 60$ deg) is up to 5.0dB.

5 Summary

In this work the body-fitted multi-block AMR method is applied to the prediction of spinning mode radiation from a generic engine exhaust with mean flow field. To model curved geometries, the AMR code is extended to support body-fitted grids. The mean flow field is assumed to be axisymmetric. Inside the duct, a spinning mode of $m = 13$ with several different radial modes ($n = 1-4$) is admitted into the propagation region as input on the boundary of the computation domain. To suppress hydrodynamic instabilities developed in the exhaust mean flow, APE are employed and are extended to the cylindrical coordinates. The results of APE agree well with the previous LEE results by comparing the near-field propagation patterns and far-field directivity. The computation efficiency varies along with the propagation of the acoustic waves. In the initial stage, the adaptively refined mesh represents a saving of up to 160% compared with a uniform mesh. After the acoustic waves spanning the whole computation domain the efficiency of AMR is the same as that on a uniformly fine mesh.

Acknowledgments

Xun Huang and Zhaokai Ma are supported by scholarships from the School of Engineering Sciences, University of Southampton. The authors would also like to acknowledge Dr X. X. Chen for helpful discussions.

REFERENCES

[1] S. K. Richards, X. X. Chen, and X. Zhang, "Parallel Computation of 3D Acoustic Radiation from an Engine Intake," AIAA Paper 2005-2947, 2005.

[2] M. J. Berger and J. Oliger, "Adaptive Mesh Refinement for Hyperbolic Partial Differential Equations," *Journal of Computational Physics*, Vol. 53, 1983, pp. 484–512.

[3] P. MacNeice, K. M. Olson, C. Mobarry, R. de Fainchtein, and C. Packer, "Paramesh: A Parallel Adaptive Mesh Refinement Community Toolkit," *Computer Physics Communications*, Vol. 126, 2000, pp. 330–354.

[4] A. Wissink and R. Hornung, "Parallel AMR Application Development with the Samrai Library," LLNL technical report UCRL-PRES-209469, 2005.

[5] X. Huang and X. Zhang, "Adaptive Mesh Refinement for Computational Aeroacoustics," AIAA Paper 2005-2873, 2005.

[6] X. Huang and X. Zhang, "Parallel Adaptive Mesh Refinement with Boundary Nonconforming Grids," Euromech Colloquium 467, Marseille, France, July 2005.

[7] X. Huang and X. Zhang, "Adaptive Mesh Refinement Computation of Acoustic Radiation from an Engine Intake," AIAA Paper 2006-2694, 2006.

[8] X. Zhang, X. X. Chen, and C. L. Morfey, "Acoustic Radiation from a Semi-infinite Duct with a Subsonic Jet," *International Journal of Aeroacoustics*, Vol. 4, No. 1-2, 2005, pp. 169–184.

[9] X. Zhang, X. X. Chen, C. L. Morfey, and B. J. Tester, "Computation of Fan Noise Radiation Through an Engine Exhaust Geometry with Flow," AIAA Paper 2003-3267, 2003.

[10] R.M. Munt, "The Interaction of Sound with a Subsonic Jet Issuing from a Semi-infinite Cylindrical Pipe," *Journal of Fluids Mechnics*, Vol. 83, 1977, pp. 609–640.

[11] R. Ewert and W. Schröder, "Adaptive Mesh Refinement for Hyperbolic Partial Differential Equations," *Journal of Computational Physics*, Vol. 188, 2003, pp. 365–398.

[12] J. E. Ffowcs-Williams and D. L. Hawkings, "Sound Generation by Turbulance and Surfaces in Arbitrary Motion," *Philosophical Transactions of the Royal Society of London*, Vol. A264, 1969, pp. 321–342.

[13] J. S. Sachdev, C. P. T. Groth, and J. J. Gottlieb, "A Parallel Solution-adaptive Scheme for Predicting Multi-phase Core Flows in Solid Propellant Rocket Motors," *International Journal of Computational Fluid Dynamics*, Vol. 19, No. 2, 2005, pp. 157–175.

[14] C. K. W. Tam and J. C. Webb, "Dispersion-relation-preserving Finite Difference Schemes for Computational Acoustics," *Journal of Computational Physics*, Vol. 107, No. 2, 1993, pp. 262–281.

[15] J. Ray, C. A. Kennedy, S. Lefantzi, and H. N. Najm, "Using High-order Methods on Adaptively Refined Block-structured Meshes - Discretizations, Interpolations, and Filters," SAND2005-7981,Sandia National Laboratories, USA, January 2006.

[16] F. Q. Hu, M. Y. Hussaini, and J. Manthey, "Low-dissipation and Low-dispersion Runge-kutta Schemes for Computational Acoustics," NASA CR-195022, 1994.

[17] C. A. Kennedy and M. H. Carpenter, "Comparison of Several Numerical Methods for Simulation of Compressible Shear Layers," NASA Technical Paper 3484, 1997.

[18] T. A. Driscoll and L. N. Trefethen, "Pseudospectra for the Wave Equation with an Absorbing Boundary," *Journal of Computational and Applied Mathematics*, Vol. 69, 1996, pp. 125–142.

[19] R. Mittal and G. Iaccarino, "Immersed Boundary Methods," *Annual Reviews of Fluid Mechanics*, Vol. 37, 2005, pp. 239–361.

[20] M. J. Berger and A. Jameson, "Automatic Adaptive Grid Refinement for the Euler Equations," AIAA Paper 1985-1633, 1985.

[21] S. K. Richards, X. Zhang, X. X. Chen, and P. A. Nelson, "Evaluation of Non-reflecting Boundary Conditions for Duct Acoustic Computation," *Journal of Sound and Vibration*, Vol. 270, 2004, pp. 539–557.

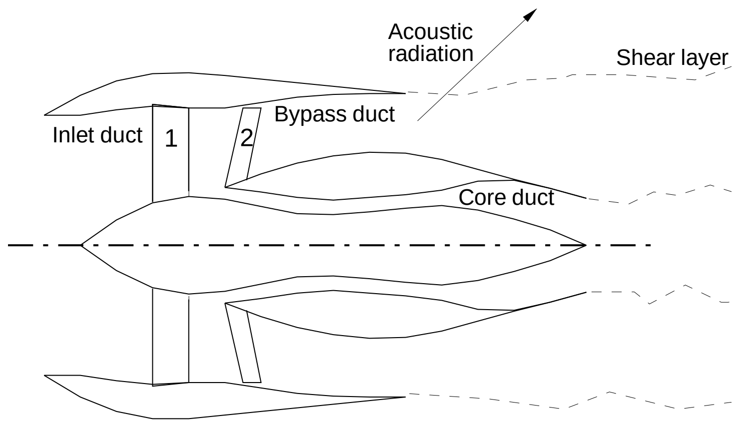

Figure 1: Tonal noise radiation off an aeroengine bypass duct, where: 1 is rotor, 2 is stator, other sectors are omitted.

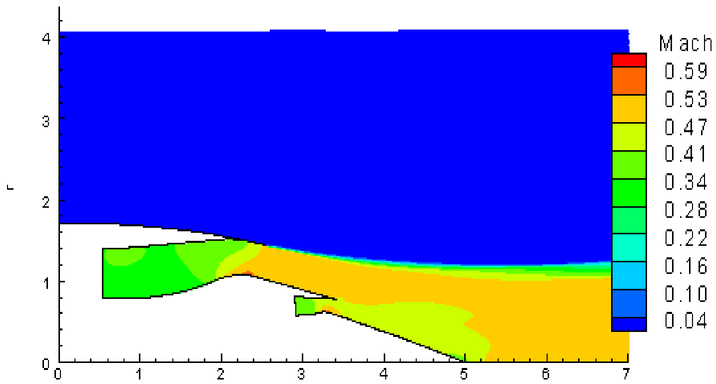

Figure 2: Mean Mach number distribution of an aeroengine exhaust.

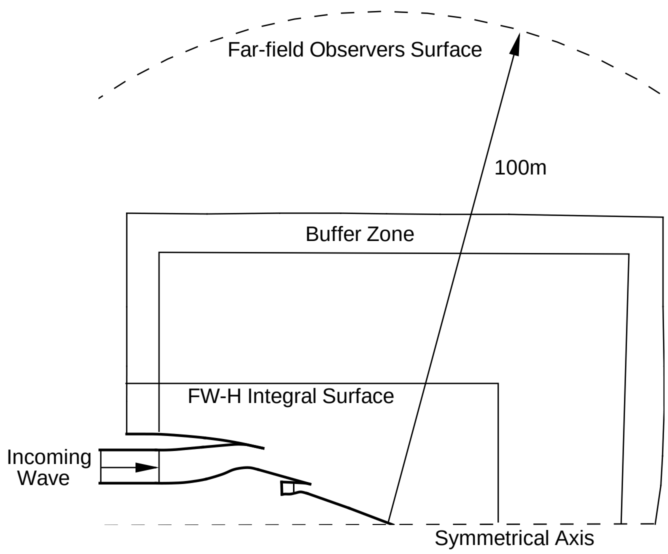

Figure 3: The problem setup of an aeroengine exhaust geometry that is displayed with thick lines.

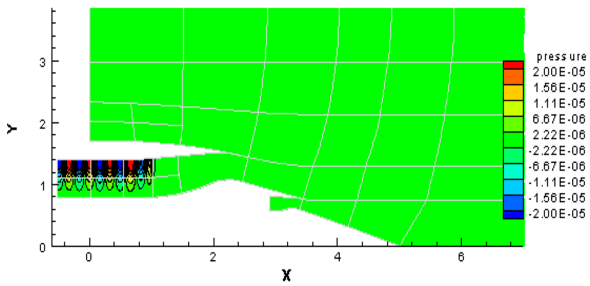

(a) $t = 1$.

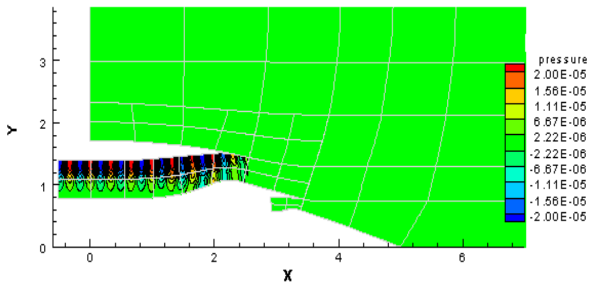

(b) $t = 2$.

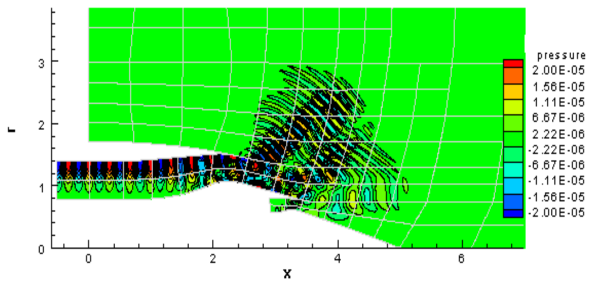

(c) $t = 4$.

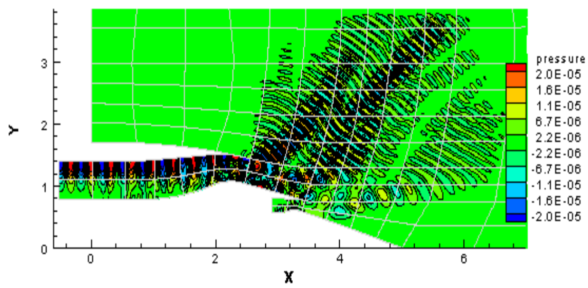

(d) $t = 6$.

Figure 4: The evolution of adaptively refined mesh with the propagation of acoustic waves from the engine exhaust. Gray lines represent the block boundaries of the adaptively refined mesh.

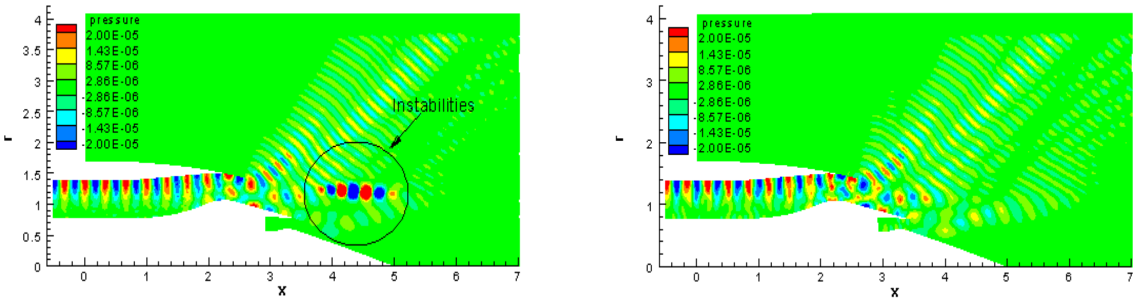

(a) LEE with AMR, $t = 12$.

(b) APE with AMR, $t = 20$.

Figure 5: Perturbation pressure contours computed by LEE and APE. $m = 13, n = 1, k = 28.3179$.

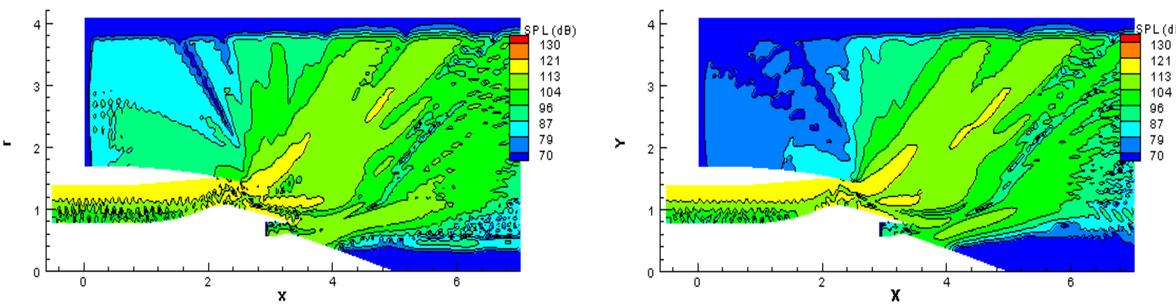

(a) LEE

(b) APE

Figure 6: SPL contours computed by LEE and APE. $m = 13, n = 1, k = 28.3179$, (a) $9.5 < t < 10$, (b) $15 < t < 15.5$.

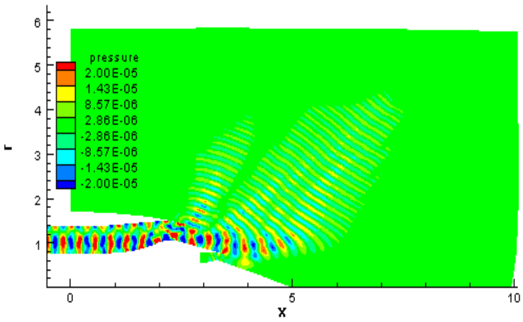

(a) Perturbation pressure, n=2.

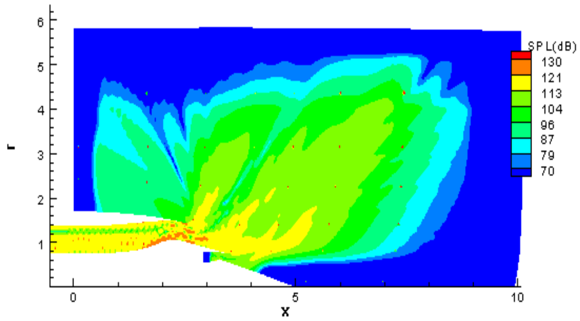

(b) SPL, n=2.

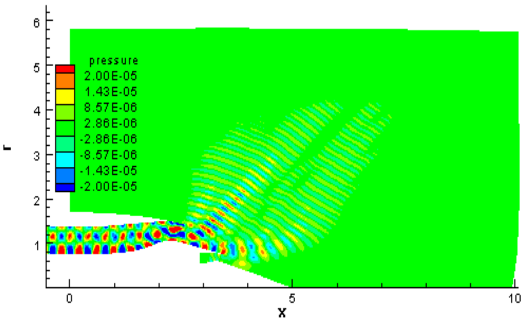

(c) Perturbation pressure, n=3.

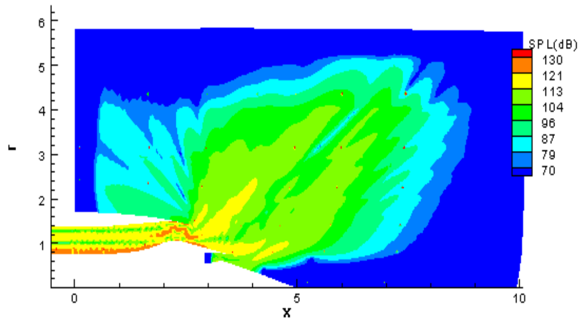

(d) SPL, n=3.

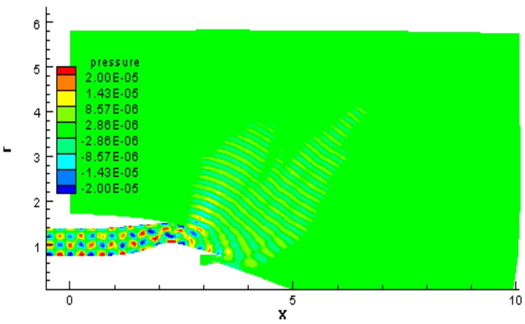

(e) Perturbation pressure, n=4.

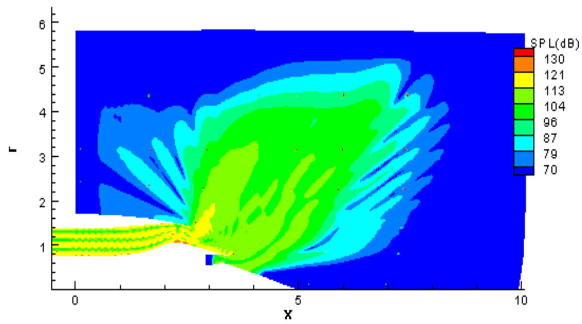

(f) SPL, n=4.

Figure 7: APE prediction of perturbation pressure and SPL contours of several single spinning mode waves. $m = 13, n = 2 - 4, k = 28.3179, 12.4 < t < 12.9$.

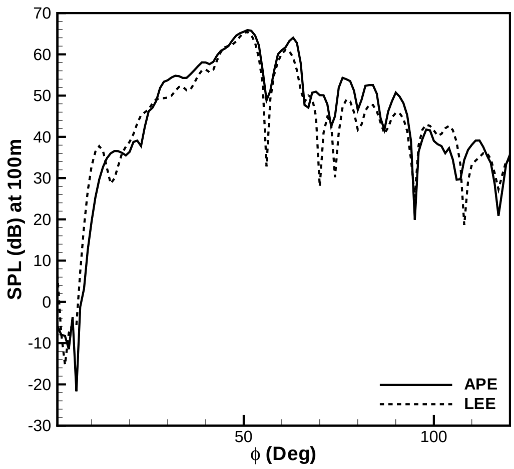

(a) $n = 1$.

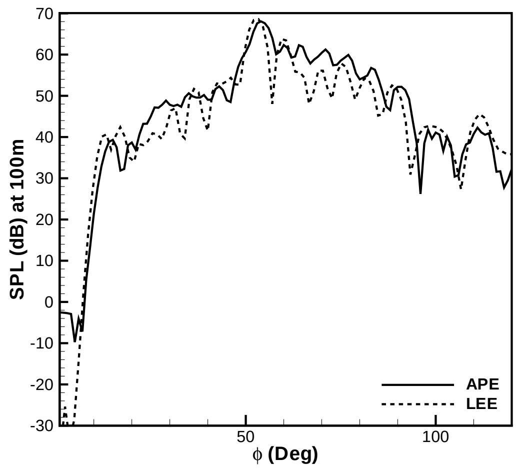

(b) $n = 2$.

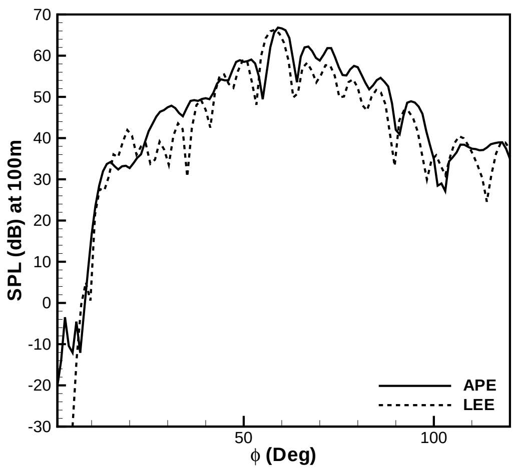

(c) $n = 3$.

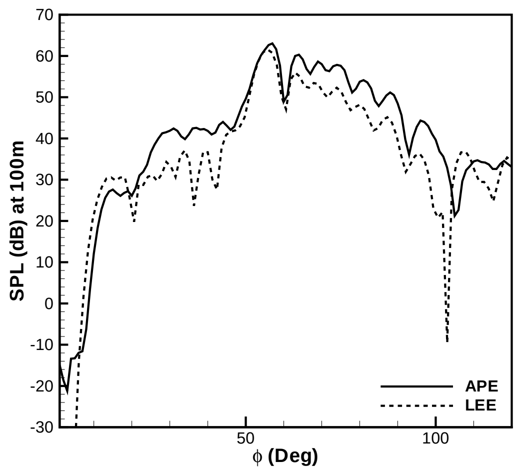

(d) $n = 4$.

Figure 8: Far-field directivity of the engine exhaust duct radiation. $m = 13, k = 28.3179$.